Primitive-Equation Instability of Wide Oceanic Rings. Part II: Numerical Studies of Ring Stability

WILLIAM K. DEWAR

Department of Oceanography, The Florida State University, Tallahassee, Florida

PETER D. KILLWORTH AND JEFFREY R. BLUNDELL

Southhampton Oceanography Centre, Southhampton, United Kingdom

(Manuscript received 10 November 1997, in final form 3 August 1998)

ABSTRACT

The study of barotropic structure and its effects on oceanic ring stability has yielded seemingly conflicting results. Some studies suggest that the stability of a given ring profile is as sensitive to the sense of the barotropic mode as it is to the vertical shear, while others suggest the vertical shear is the sole dominant effect. Here numerical evidence that supports both views is presented. Warm rings with a favorable barotropic structure can retain their monopole nature while cold rings do not. These results are of interest given the observed long lifetimes of oceanic rings.

As evidence a series of initial value integrations is presented. The initial ring profile consists of an exponential profile decaying as the cube of the radial distance, rather than as the squared decay law of the commonly used Gaussian. The reasons for this choice are that previous studies have examined the Gaussian initial condition extensively and recent analysis suggests the Gaussian profile has special stability properties.

The authors find that the barotropic mode affects the coherence of warm rings, yielding essentially stable, monopolar structures for the case that the initial deep flow is in the same sense as the surface flow (i.e., in the ''co-rotating'' case), even if the initial underlying ring is linearly unstable. Thus, warm rings remain dominantly monopolar, although an underlying, weak tripole is often seen in the final state. Cold rings in the oceanic parameter regime, on the other hand, experience no such stabilizing effects from deep structure. Quasigeostrophic dynamics fails to capture the stabilization tendencies of warm rings with corotating deep flow, suggesting the effect is related to the finite-amplitude thickness changes of a warm ring. The transition from an unstable, warm monopolar initial state to an effectively stable, warm initial monopolar state is a sensitive function of the barotropic mode. Finally, beta-plane experiments demonstrate the robustness of the primitive equation result.

Thus, it is suggested that the barotropic component of a warm ring can enhance ring stability as a monopole by providing for the existence of a nearby tripolar state to which the ring evolves and thereafter remains. The observed stability of cold rings, however, remains a mystery.

1. Introduction

Gulf Stream rings and Agulhas rings are well-known oceanic manifestations of coherent vortices whose lifetimes can be of order years. Although the observational record supporting ring longevity is quite clear, the dynamical underpinnings for this are not. The observed baroclinic structure of such rings is often, if not always, dominantly monopolar and they are routinely of a radial scale that is large compared to the deformation radius. One generally expects such structures to be unstable and, indeed, this result is found in many linear stability studies. Of course, this is at odds with the observations. Here we attempt to bridge the gap between these disparate results by numerical investigation and support the premise raised elsewhere that the stability of warm rings is a strong function of their ''barotropic'' component. If surface and deep flows are in the same sense, ring stability is enhanced in that, even for a linearly unstable profile, a nearby dominantly monopolar state can exist that is stable and attracts the evolution of the ring.

Background

The remarkable stability of oceanic rings is no longer seriously debated. The multiyear lifetimes of rings were first documented for cold Gulf Stream rings by Lai and Richardson (1977) by analysis of in situ observations. Brown et al. (1986) analyzed the longevity of warm Gulf Stream rings using satellite infrared SST imagery.

Corresponding author address: Dr. William K. Dewar, Department of Oceanography, The Florida State University, Tallahassee, FL 32306-4320.

Gordon and Haxby (1990) argue that Agulhas warm rings can live up to seven years during which time they can cross the entire South Atlantic in a trajectory of possible importance to global climate.

The hydrographic structure of rings is also well known and routinely consists of a single extremum in isopycnal depth, with cold eddies containing a shallow thermocline and warm eddies a deep thermocline. The amplitude of the maximum isopycnal depth anomaly is generally 500–700 m (The Ring Group 1981; Olson et al. 1985; Olson and Evans 1986). The lateral dimensions of rings are also interesting. Based on hydrographic data, reduced gravity parameters have been estimated for warm Gulf Stream rings (Olson et al. 1985) and warm Agulhas eddies (Olson and Evans 1986). These yield deformation radius estimates for the eddies, and in both cases it was found the rings were roughly six deformation radii in diameter. Since length scales routinely appear in dynamical theories as the square of their ratio to the deformation radius, this implies that long-lived rings are ''large.''

In contrast, the velocity structure of rings is less well known and is possibly quite variable. The generic picture of warm Gulf Stream rings is that they are dominantly monopolar, although smaller-scale ringlets are often observed on their periphery (Kennelly et al. 1985; Hooker et al. 1995). Agulhas eddies are also often apparently monopolar, although it is not unusual for an oppositely rotating vortex to appear near them. Regarding the vertical distribution of momentum in rings, data suggest they often possess deep velocity signatures. This is supported by the reduced gravity fits of Olson et al. (1985) and Olson and Evans (1986) and that surface-tracked rings exhibit trajectory anomalies in the vicinity of deep topography irregularities. Chassignet (1990) also found the rings formed in his Agulhas Current system model naturally developed deep velocity signatures as a result of their formation. Killworth's (1992) analysis of the FRAM model results showed that an approximately equivalent-barotropic vertical distribution accounted for most of the energy in both mean and fluctuating components of the horizontal flow field.

The observed long ring lifetimes have encouraged the study of ring stability. Examinations of compensated (no deep flow) monopolar eddy structure using primitive equation dynamics have routinely revealed linear vortex instability (Paldor and Nof 1990; Ripa 1992). In quasigeostrophic (QG) studies, Ikeda (1981) found increasing growth rates for vortex linear instabilities with increasing shear, in keeping with the overall baroclinic instability of his profiles. Helfrich and Send (1988) and Flierl (1988) argue that QG vortices of increasing size are increasingly unstable, with the dominant instabilities at wavelengths of the deformation radius. They also suggest that deep flows, when in the same sense as the surface flows, can reduce the growth rate amplitudes.

In a primitive equation study of linear vortex instability, Dewar and Killworth (1995, hereafter DK) argued that the sense of the deep flow was a determining factor in the stability of a warm vortex. Using a Gaussian profile in both layers, and with a lateral scale large compared to the deformation radius, they frequently could find no unstable normal modes in the case where the deep flow and surface flows were in the same sense (the ''co-rotating'' case). The other cases of compensated and counterrotating warm eddies were strongly baroclinically unstable, thus they suggested the nature of the deep flows under rings were of fundamental importance to ring stability. Numerical initial value integrations on f and β planes supported the relevance of the linear analyses into the nonlinear regime.

The DK results, however, are seemingly at odds with analyses of broad parallel shear flow. Killworth (1980) demonstrated by a slowly varying analysis that such flows were routinely unstable to disturbances on the deformation scale. Helfrich and Send (1988) and Flierl (1988) argued as much for QG vortices. More recently, Benilov et al. (1997) have argued that geostrophic rings are, regardless of profile, all unstable, and that those studied in DK were unstable to non-normal model disturbances. The latter point suggests why the normal mode linear stability study performed in DK failed to find any unstable modes for their ring.

Thus, Killworth et al. (1997, hereafter KBD) revisited the instability problem by means of an asymptotic analysis in the limit of large rings. Three results relevant to this paper were found. First, the Gaussian profiles studied by DK were found to be special in that in the QG limit, the location of the instability occurred at the origin, but the slowly varying theory was not valid there. In this paper, we therefore study a ring initial profile, other than Gaussian, which does not suffer from this consideration. Second, for large radially symmetric ring profiles other than Gaussian, the instability problem was shown analytically (by means of a slowly varying analysis) to behave like the classical baroclinic parallel shear-flow instability problem and was relatively insensitive to the barotropic component. This result is at odds with the Gaussian eddy analysis in DK. Last, when the linear eigenvalue problem was solved numerically (i.e., without appealing to the approximations inherent in the asymptotic analysis), radially symmetric profiles in general proved to be unstable. Sometimes the dominant instability was that given by the asymptotic analysis, for example, for cold core rings; sometimes it was not (in the case of warm rings). This is in agreement with the analysis of Benilov et al. (1997).

In summary, the linear stability of wide oceanic rings is at odds with observations. Specifically, they are generally linearly unstable, which leaves unanswered the question of how they can survive for periods close to a decade. Further, the linear stability results of DK possibly reflect properties special to the Gaussian profile. Regarding the numerical initial value results in DK, we are then left with two alternative possibilities. First, the apparent stability at finite amplitude of the Gaussian

vortex could be a result as special as its linear stability. Second, the apparent stability of the Gaussian is representative of a general finite amplitude trend. This latter possibility is suggested by the results of Carton and McWilliams (1989) from QG experiments. (Note that finite amplitude stability of the ring profiles has not been widely examined.)

Here, the effect of corotating versus counterrotating or compensated structure on ring stability is again investigated with a view to distinguishing between the above two possibilities. The hypothesis behind the experiments is that the latter of the two above possibilities holds; namely, that how ''far'' a vortex may evolve away from its initial state is a strong function of its deep flow. For warm rings, we find that if the structure is corotating, the final state to which the vortex evolves tends to be ''close'' to the initial state, while for compensated and counterrotating eddies, complete destruction of the monopolar initial eddies can often ensue. Thus, we in some sense extend the Carton and McWilliams (1989) result into the regime of primitive equation dynamics, while at the same time emphasizing the dependence of this equilibration mechanism on the deep flow of the ring. Numerical experiments with cold rings, on the other hand, demonstrate instability regardless of deep flow.

Most of our results come from numerical experiments using primitive equations on the f plane. However, we have also looked into a number of other effects to assess the generality of the results. Specifically, we present evidence that quasigeostrophic dynamics fails to capture the stabilizing effect of deep flow on warm rings and that the presence of beta does not disrupt the stability properties of warm rings.

Also, we find the transition between ''unstable'' and ''stable'' warm eddies to be surprisingly abrupt. Small changes in the ratio of deep to surface flow can produce drastically different results. Large counterrotating eddies fragment into smaller dipoles and scatter, while large corotating eddies develop weak tripolar structure, and remain dominantly monopolar. Further, this behavior occurs in a parameter regime typical of oceanic rings. Thus, we suggest knowledge of the deep flow in warm rings is essential to gauging their overall stability.

A brief review of the linear stability analysis is provided in the next section. Our warm ring numerical experiments are described in section 3 and results are given. Section 4 describes our β-plane, cold ring, and quasigeostrophic experiments, and the paper ends with a discussion and conclusion.

2. Linear stability analysis

Consider a radially symmetric Boussinesq vortex on an f plane (see Fig. 1). The two-layer, flat-bottomed equations governing this system are

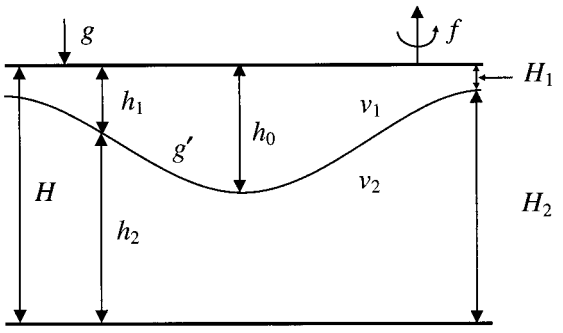

FIG. 1. System schematic: A two-layer primitive equation f-plane system is considered, and the Boussinesq assumption is employed. The system is assumed to have a flat bottom and notation is standard.

$$u_{jt} + u_j u_{jr} + \frac{v_j u_{j\theta}}{r} - \frac{v_j^2}{r} - f v_j = -P_{jr} \qquad (1)$$

$$v_{jt} + u_j v_{jr} + \frac{v_j v_{j\theta}}{r} + \frac{u_j v_j}{r} + f u_j = -\frac{P_{j\theta}}{r} \qquad (2)$$

$$h_{jt} + \frac{1}{r}(r u_j h_j)_r + \frac{1}{r}(h_j v_j)_\theta = 0, \qquad (3)$$

where j (=1, 2) is a layer index (numbered downward), u_j represents radial velocity, v_j azimuthal velocity, t time, r radial coordinate, θ azimuthal coordinate, P_j pressure divided by mean density, f the Coriolis parameter, and h_j the thickness of the jth layer. Subscripts r, θ, and t denote differentiation. Layer pressures and thicknesses are connected by the hydrostatic relation and the constant depth; namely,

$$P_1 - P_2 = g'(h_1 - H_1); \qquad h_1 + h_2 = H, \qquad (4)$$

where g' is the reduced gravity parameter associated with the interface, H_1 is the upper-layer thickness at large radius, and H is the total fluid depth.

KBD proceed by nondimensionalizing (1)–(3) according to a length scale L and a velocity scale connected to L via

$$U = \frac{g' H_1}{fL}.$$

The result is

$$\frac{g' H_1}{f^2 L^2}\left(u_{jt} + u_j u_{jr} + \frac{v_j u_{j\theta}}{r} - \frac{v_j^2}{r}\right) - v_j = -p_{jr} \qquad (5)$$

$$\frac{g' H_1}{f^2 L^2}\left(v_{jt} + u_j v_{jr} + \frac{v_j v_{j\theta}}{r} + \frac{u_j v_j}{r}\right) + u_j = -\frac{1}{r} p_{j\theta} \qquad (6)$$

$$h_{jt} + \frac{1}{r}(r h_j u_j)_r + \frac{1}{r}(v_j h_j)_\theta = 0, \qquad (7)$$

and (4) becomes

$$P_2 = P_1 - (h_1 - 1), \qquad h_1 + h_2 = 1 + \delta^{-1}, \qquad (8)$$

where $\delta = H_1/H_2$ is the depth ratio of the two layers

based on their undisturbed thicknesses at large r. The analysis in KBD proceeds by linearizing (5)–(7) about the basic state defined by the pressure field

$$\overline{P}_j = E_j e^{-r^3} \tag{9}$$

with velocities determined via a cyclostrophic balance. The usual normal mode solution forms for the perturbations are used; that is,

$$P_j', h_j', u_j', v_j' \sim e^{in(\theta - ct)}. \tag{10}$$

The previously discussed observations suggest the analysis of these equations in the limit of large eddies. In particular, Olson and collaborators argue

$$\varepsilon^2 = \frac{g' H_1}{f^2 L^2} \ll 1$$

for both Gulf Stream and Agulhas rings. Note that the smallness of this parameter implies that relative vorticity is weak. Potential vorticity in each layer is thus dominated by thickness, ensuring all the eddies are potentially baroclinically unstable because of the necessary reversal with depth of the potential vorticity gradient. In any case, (5)–(7) were solved analytically in KBD by an expansion in ε. Of more immediate relevance to this study, they also considered the numerical solution of (5)–(7) using a numerical shooting method.

Parameter values

We will always assume a constant depth ocean of 4000 m and use a Coriolis parameter of 0.93×10^{-4} s^{-1}. In our warm rings experiments, the other parameters are typical of field observations and come from DK; namely, the far-field depth will be 40 m and the central depth will be 520 m. Thus, our depth ratio $\delta = H_1/H_2 = 0.0101$. The reduced gravity parameter used here is $g' = 1.06 \times 10^{-2}$ m s^{-2}, as suggested by the fit in Olson et al. (1985) to warm core ring 82B. Dewar and Killworth examined Gaussian eddy profiles with a decay scale of 84 km. Here, we will examine exponential cubic structures as in (9), but will retain the same length scale, $L = 84$ km. With these parameters, $\varepsilon \sim 1/12 \ll 1$. The central upper-layer thickness of the eddy is written [see (8)] as

$$h_o = 1 + E_1 - E_2, \tag{11}$$

where the subscript 1 has been dropped.

Given that the baroclinic structure is well known for rings but the depth-averaged velocity structure is not, we have varied the E_j layer pressure amplitudes in (9) by amounts independent of j, that is, $E_1 = E_T + \Delta E/2$, $E_2 = E_T - \Delta E/2$ for fixed ΔE (here we will often use $\Delta E = 12$, which amounts to a total central eddy depth of 520 m). This fixes the thermocline structure according to (11) (resulting essentially in a fixed vertical shear) but allows the absolute layer velocities to span a range of values. Thus, a choice $E_T = \Delta E/2$ results in a compensated eddy structure with no lower-layer flow. Larger values of E_T produce lower-layer flows in the same sense as the surface (the corotating case) and smaller E_T yield surface and deep flows in opposite senses (the counterrotating case). With n in (10) as a free parameter, the eigenvalue routine can be used to extract both eigenfunctions and complex growth rates. We have generally found the azimuthal values $n = 2$ or 3 to yield the largest growth rates.

We have performed a series of numerical experiments that test the KBD eigenmode solutions. Specifically, we have employed a version of the Miami Isopycnic Coordinate Ocean Model (MICOM) (Bleck and Chassignet 1994) in a two-layer format to conduct the experiments. The equation solved by the MICOM model is essentially like (1)–(3), although they are written in a Cartesian, rather than a cylindrical, coordinate system. The basic pressure field was specified according to (9). We then added small perturbations in the form of the unstable eigenmodes to the initial state and carried out initial value calculations. Corresponding initial value calculations with unperturbed vortices were also carried out. The results from these two sets of experiments were differenced at given intervals to yield views of the evolution of the perturbations. All computations used a grid spacing of 5 km, 201 grid points in each direction and free slip boundary conditions. Most of the experiments shown here used a lateral viscosity of 100 m^2 s^{-1}, although we have investigated the sensitivity of our results to viscosity by conducting a smaller number of experiments using viscosity values of 20 m^2 s^{-1} and 10 m^2 s^{-1}. These results support our contention that our major results do not depend on viscous effects.

A typical result of this procedure appears in Fig. 2. The parameters of this run were $E_1 = 18$, $E_2 = 6$; that is, the eddy is strongly corotating. It was found that the $n = 2$ eigenmode for this system was the most unstable. The structure of this eigenmode in upper-layer thickness effectively appears in Fig. 2a, which shows day 4 of the numerical integration. The subsequent panels in Fig. 2b and 2c show the perturbation at 4-day intervals, as calculated by the model. Note that the shape of the perturbation is largely unchanged during this integration, although the amplitude grows and the mode swirls anticyclonically around the vortex.

The eigenvalue routine returns a nondimensional value of $c_r = -2.99$ for the angular velocity and $nc_i = 3.3$ for the growth rate. The negative value of the former implies the anticyclonic motion of the eigenmode. The timescale associated with the parameters in use is 17.9 days; thus, the above values correspond to an eigenmode turn over a timescale of 37.5 days and a growth timescale of 5.43 days. Over the 8-day span portrayed in Fig. 2, these values predict a movement 77° and an increase in the eigenvector amplitude by a factor of $e^{(8./5.43)} = 4.36$. In comparison, the eigenmode in Fig. 2 moves roughly 78° and increases in amplitude from a maximum of roughly 5 m to a little more that 21 m, in

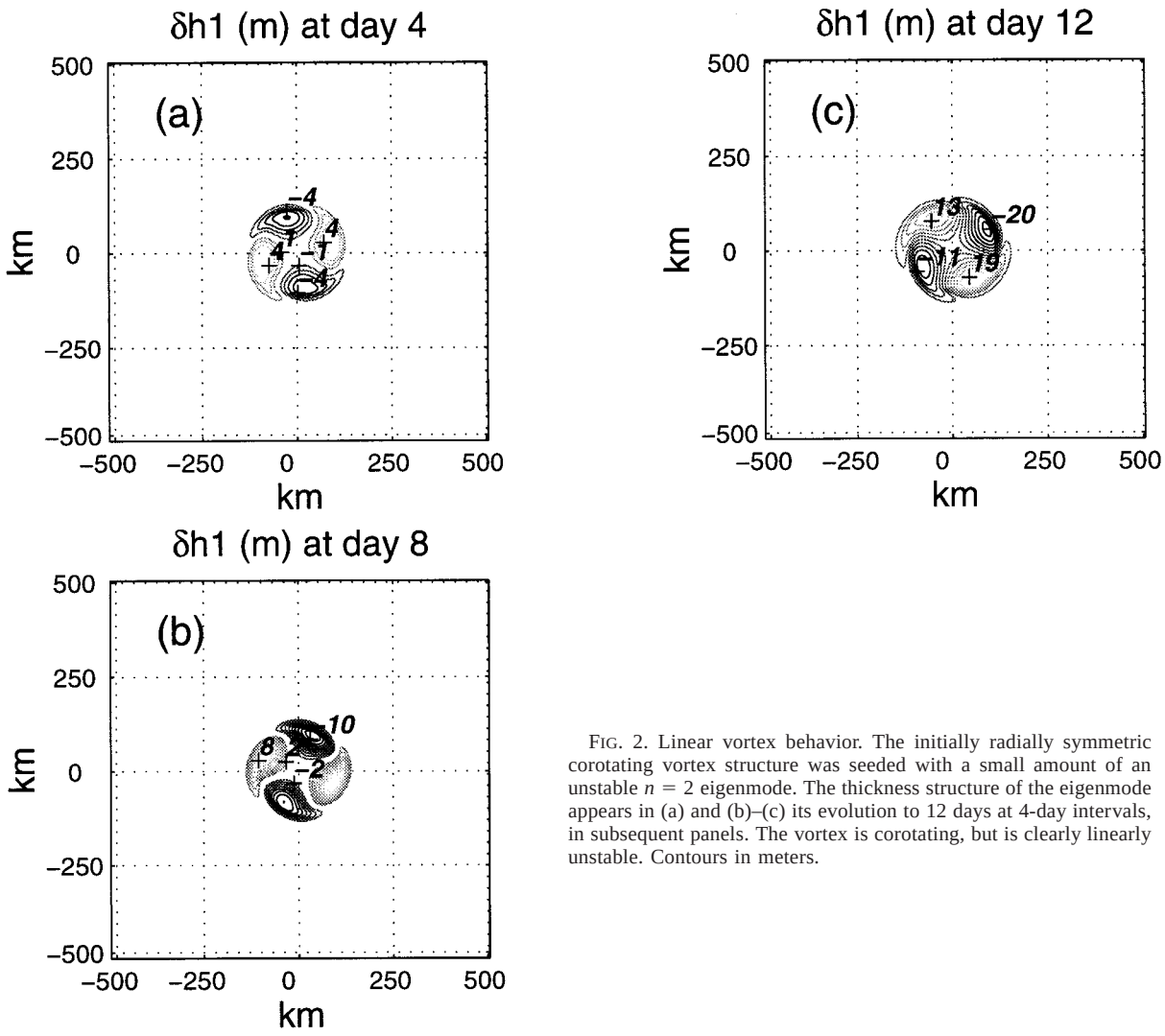

FIG. 2. Linear vortex behavior. The initially radially symmetric corotating vortex structure was seeded with a small amount of an unstable $n = 2$ eigenmode. The thickness structure of the eigenmode appears in (a) and (b)–(c) its evolution to 12 days at 4-day intervals, in subsequent panels. The vortex is corotating, but is clearly linearly unstable. Contours in meters.

agreement with the predictions of the instability theory. Such comparisons are typical of several we have made in the linear regime.

3. Finite amplitude results

The previous section demonstrates that the cubic exponential profile is linearly unstable in the corotating regime and, as such, contradicts the suggestion in DK that corotation could generally suppress vortex instability. This is also in agreement with the results of Benilov et al. (1997). On the other hand, consider the comparison shown in Fig. 3. Figure 3a shows the upper-layer thickness initial condition for three experiments. The full initial condition consists of our standard 84-km cubic exponential profile for the thermocline and its associated cyclostrophic shear velocity fields. The full velocity includes a cyclostrophic contribution from the free surface pressure gradient. These fields were seeded with small additions of fastest growing linear normal modes (see below). The amplitude of the perturbations were the same in all experiments. Other parameters, like resolution and viscosity, are identical to those in the previous section.

Figures 3b–d show the upper-layer fields from three of our experiments; Fig. 3b is at day 40, 3c is at day 60, 3d is at day 100. There are two differences between these initial value experiments. First is the values assigned to E_T; the results in 3b used $E_T = 0$, those in Fig. 3c used $E_T = 6$, and those in Fig. 3d used $E_T = 12$. Thus, the state shown in 3b is the result of a counterrotating experiment, that in Fig. 3c comes from a compensated experiment, and that in Fig. 3d comes from a corotating experiment. The second difference is that the fastest growing normal-mode perturbation used to seed each initial value was that appropriate to the particular E_T value. We have performed several such numerical experiments in the counter-, compensated, and

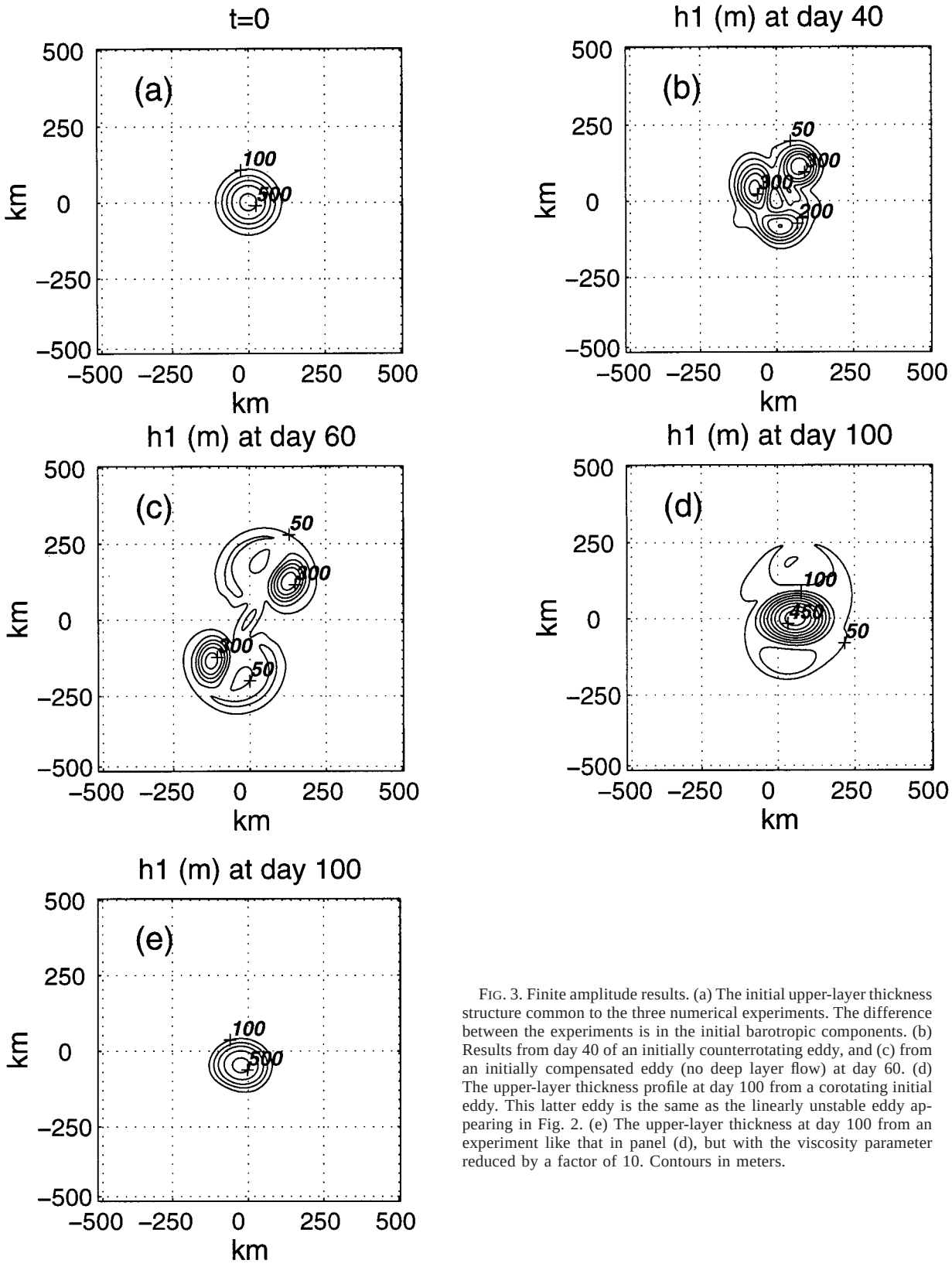

FIG. 3. Finite amplitude results. (a) The initial upper-layer thickness structure common to the three numerical experiments. The difference between the experiments is in the initial barotropic components. (b) Results from day 40 of an initially counterrotating eddy, and (c) from an initially compensated eddy (no deep layer flow) at day 60. (d) The upper-layer thickness profile at day 100 from a corotating initial eddy. This latter eddy is the same as the linearly unstable eddy appearing in Fig. 2. (e) The upper-layer thickness at day 100 from an experiment like that in panel (d), but with the viscosity parameter reduced by a factor of 10. Contours in meters.

corotating regimes; those discussed here exhibit typical behavior characteristics of each of these categories.

Consider first the counterrotating behavior in Fig. 3b, for which $(E_1, E_2) = (6, -6)$. This is typical of the behavior of all experiments in which the initial sense of the deep flow was counter to the surface flow. The linear instability grows until nonlinear behavior sets in, soon after which the fields bear no resemblance to their initial structure.

The compensated behavior in Fig. 3c, for which $(E_1, E_2) = (12, 0)$ is similar, in that it too breaks apart from its original monopolar state. It is less unstable than the counterrotating ring, in that the time necessary for the initial vortex to degenerate into a multipolar state is increased as the vortex is moved toward the corotating state. (Recall that the snapshot in Fig. 3b is from day 40, earlier than the day 60 result in Fig. 3c.) We do note however that the counterrotating experiment has degenerated into three centers. These subsequently remain close to each other for the duration of the experiment (100 days), but do not coalesce. In comparison, the compensated state has generated two dipoles, which thereafter move apart. In this sense, the ''less'' unstable compensated initial state suffers a more catastrophic fate than the ''more'' unstable counterrotating state. This distinction does not characterize the β-plane results, however.

The profile in Fig. 3d, for which $(E_1, E_2) = (18, 6)$, has also evolved, but it is clear also that it is dominantly a monopole and thus much closer to its initial state. Recall also that this profile $(E_1, E_2) = (18, 6)$ was used in the previous section to establish the general linear instability of the cubic exponential in the corotating regime. Continuation of the above run beyond 100 days establishes that the monopole in (c) is subject at best to slow evolution.

Figure 3e shows the results at day 100 from an experiment essentially like that shown in Fig. 3d. The only difference is that in this run, the value of the viscosity was reduced from 100 to 10 $m^2 s^{-1}$. Note that the overall structure of the thermocline profile is unchanged by this parametric modification, suggesting that no weak instabilities have been damped by viscosity. Thus, we argue that the corotating structure in Fig. 3d is effectively stable.

The above results hint at a role for the deep flow in setting the stability characteristics of vortices. Namely, a corotating monopolar state, although linearly unstable, can apparently evolve to a nearby essentially monopolar state that is stable. Further, the difference between Fig. 3c and Fig. 3d demonstrates that this capacity is a function of E_T, which we here refer to as the barotropic vortex component.

a. Sensitivity to E_T

We here examine how the stability of a warm ring depends on E_T and offer numerical evidence that the final state achieved by a ring is a surprisingly sensitive function of this parameter. We again consider the evolution of our standard system from three initial (perturbed) thermocline states (rather as in Fig. 2a, but with differing E_T values, all in the corotating regime). The plots in Figs. 4a,b—experiment 1—employ $(E_1, E_2) = (13, 1)$, those in Figs. 4c,d—experiment 2—employ $(E_1, E_2) = (13.75, 1.75)$, and those in Figs. 4e,f—experiment 3—employ $(E_1, E_2) = (14, 2)$. Thus, we examine the consequences of an increasing corotating deep flow, although the change in deep flow is slight. For example, the difference in the swirl velocity in the latter two experiments is less than 0.02 m s^{-1} (cf. typical upper-layer swirl velocities of 0.75 m s^{-1}). Results at days 60 and 80 are shown in Figs. 4a,b and 4c,d, while results at days 80 and 100 appear in 4e,f. Note the qualitative similarity in the upper panels from all three experiments (Figs. 4a,c and 4e), in that all vortices are characterized by a strong second azimuthal mode contribution. This is indicative of the similar properties of the linearly unstable eigenmodes of all three nearby initial states.

The interesting result emerges upon comparison of Figs. 4b,d and 4f. Note that the monopolar vortex in the first two experiments has split into two dipoles, which subsequently separate; thus complete destruction of the vortex occurs. In contrast, the vortex in Fig. 4f rebounds into a dominantly monopolar structure, which therefore resembles its initial state. Further, this profile subsequently remains coherent, as is evidenced in Fig. 4g, where the structure from the last experiment at 160 days is shown. Clearly, the fundamental evolution of the system has been drastically altered by this rather minor modification of E_T, occurring somewhere between $(E_1, E_2) = (13.75, 1.75)$ and $(14.0, 2.0)$.[1] It is also interesting that experiments with stronger initial barotropic components exhibit qualitatively the behavior shown in Figs. 4f,g; that is, an essentially monopolar state results from the nonlinear evolution of the system. Figure 3c provides an example.

The mechanism by which this stabilization occurs is not clear, although there are some interesting tendencies. Most important is that upon closer inspection, one finds evidence of a weak tripolar field with a barotropic expression in the evolved final state. This appears in the thermocline structure in Figs. 4f,g in that the thermocline has an $n = 2$ azimuthal mode component. Figure 5 shows velocity vector plots at day 160 (i.e., corresponding to Fig. 4g) from both layers, which also supports the tripolar structure and similar results were seen for the (18, 6) eddy shown in Figs. 3d,e. Velocity vectors from every third point are shown, and the amplitude of vectors in the top layer (Fig. 5a) greater than 0.25 m

[1] There is evidence of mode changes in KBD's Fig. 4b as the system passes from counter- to corotating, but no obvious changes occur precisely at these parameter values.

s^{-1} has been truncated to 0.25 m s^{-1}, with a similar truncation to 0.05 m s^{-1} in the lower layer (Fig. 5b). The truncation is designed to emphasize the presence of a tripolar structure beyond the central vortex, which, though weak, will prove of importance below.

The tripolar structure is seen in the presence of the two cyclones occurring roughly with the weak neighboring thermocline extrema seen in Fig. 4f,g. In addition, these cyclones rotate along with the main vortex, during which their spatial coincidence with the thermocline centers is preserved. This is worth mentioning because Fig. 5 also shows the presence of other features in the velocity field. These other features do not retain their coherence with the main anticyclone, as do the indicated cyclones. Also, the appearance of the cyclones in both layers supports the barotropic expression of the tripole.

Although the final apparently stable structure appearing in Figs. 4f,g and Fig. 5 is no longer strictly a monopole, it is clear that the thermocline expression of the neighboring cyclones is quite weak compared to that of the main anticyclone. It is for this reason that we identify the evolved state as being close to its initial strictly monopolar initial condition. Carton and McWilliams (1989) also found in an investigation of quasigeostrophic monopolar vortices of arbitrary exponential structure that unstable vortices could evolve to a nearby tripolar state.

Considerable evidence exists to suggest that barotropic tripoles, like dipoles, are very stable. This is seen in the laboratory experiments of Kloosterziel and Van Heijst (1989). We speculate that in our experiments here, increasing the barotropic component of the vortex has altered the phase space of this system to the point where it falls into the attracting basin of a nearby tripole. It is interesting that this occurs preferentially in the corotating regime and also that this barotropic mechanism can overcome the baroclinic mechanisms, which in all likelihood are capable of driving vortex instability.

b. Linear stability of symmetrized eddies

The stabilized slightly tripolar eddies we have studied were sufficiently ''near'' radial symmetry to prompt an examination of their apparent linear stability, with or without their interactions with the mode-2 riders, rather as carried out by Carton and McWilliams (1989) in the QG limit. A symmetrization process was carried out by taking the mean azimuthal velocity fields at each radius (measured relative to the centroid) and fitting them with splines, followed by deriving the h and P field from cyclostrophy. This would create, at our choice, either an exact fit to the symmetrized depth profile or a smoothed version of the profile (in fact, exact fits yielded weak and noisy instabilities, with c_i of order 0.09 or less, and are not considered further). The symmetrized velocity fields were created by requiring cyclostrophic balance to hold.

Figure 6 shows the resulting upper depth field for the symmetrized eddy (at day 160), which was initially (14, 2), compared with the initial depth structure, and also an approximate analytical fit to the profile of the form

$$\overline{P}_j = E_j \exp(-r^p) + \gamma_j \exp[-(r - r_{cj})^2/w^2], \quad j = 1, 2,$$

where $p = 2.39$ is smaller than the initial value of 3 and the width w of the Gaussian tail is 0.5.[2] It is clear from either version of the depth field that upper-layer mass has systematically moved outward radially between the initial configuration and the final symmetrized one, with the Gaussian ''humps'' containing much of the missing part of the initial mass field. These humps are almost certainly related to the tripolar structure observed.

Again, we stress that the potential vorticity profiles of these eddies all meet the necessary conditions for instability provided by quasigeostrophic theory. This is due to the fact that the eddy thickness dominates the layer potential vorticities. Recall that the large length scales of the eddies renders relative vorticity a weak effect [see (5) and (6) and the following discussion]. Since the total depth is constant, the thickness gradients reverse with depth, implying all the eddies are potentially baroclinically unstable.

The symmetrized eddy was found to be very (linearly) stable, with growth rates of at most $c_i = 0.05$ (and again noisy). This can be compared with the initial (14, 2) eddy, which for wavenumber 2 had $c_i = 0.682$, corresponding to a growth rate of 1.36. However, with the Gaussian humps removed, the eddy became unstable once again for wavenumber 2, with $c_i = 0.34$, half of the original rate. Similar calculations on the approximate analytical fit produced $c_i = 0.28$, which is less than half the initial value, but still significantly unstable; removing the Gaussian humps increased c_i to 0.36, similar to the splined case.

These calculations demonstrate two facts: First, the results are remarkably sensitive to the depth distribution used; eddies differing by amounts less than the variability inherent in the symmetrization process (i.e., the variability in any estimate from observations, say, which involve an explicit symmetrization) have growth rates differing by orders of magnitude. Second, restricting attention to the splined fits to the profile, the eddy itself is very stable, and the stability is produced by the presence of the Gaussian humps.

These results suggest a persuasive picture of a slumping of the initial eddy induced by its own instability into a stable, nearly symmetric eddy [in disagreement with Carton and McWilliams (1989)]. However, similar tests on the symmetrized form of the (18, 6) eddy (which

[2] This fit is equivalent-barotropic (apart from the Gaussian humps); a slightly better fit can be obtained by relaxing this assumption.

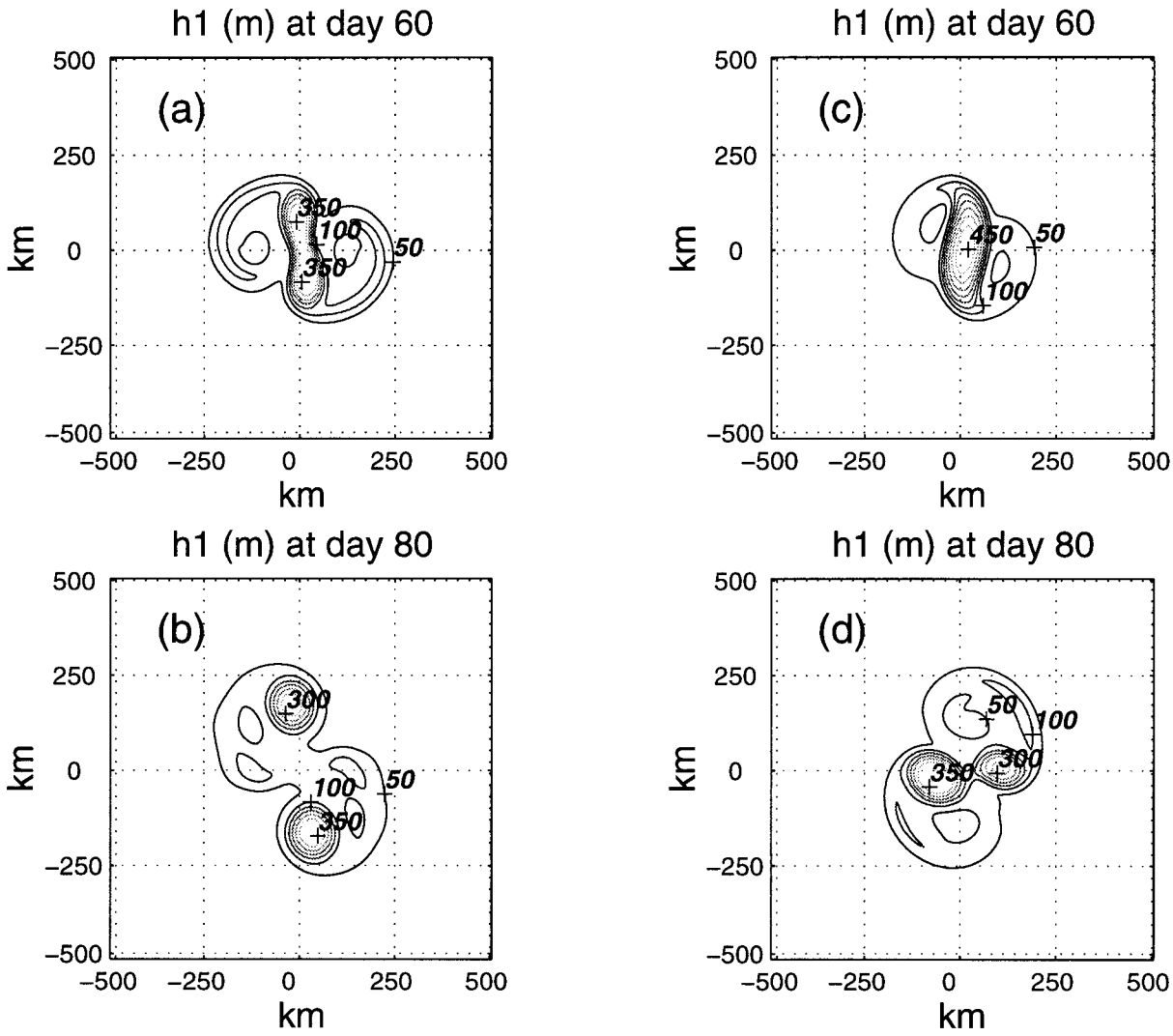

FIG. 4.

also stabilized), do not completely support the conclusion; linear stability calculations gave a c_i at 0.19 compared with the initial c_i of 1.65, a reduction by a factor of 8. Thus in this case instability remains, but at a much weaker rate than for the initial profile.

Linear stability calculations should, of course, be made for the actual precessing tripolar structure rather than a pure radial structure. Such a calculation is complicated since there are interactions between riders and the growing mode, which, given the same azimuthal mode-2 structure, could either act to stabilize or destabilize. We are forced to conclude that the presence of azimuthal structure is important in determining the stability, or otherwise, of the collapsed eddies. We suspect, too, that cancellation between barotropic and baroclinic components of the energy budget, rather as in DK, may be playing a part. The initial profiles discussed here all have roughly equal contributions by barotropic and baroclinic interactions. The (18, 6) symmetrized case also has contributions that are about equal. The (14, 2) symmetrized eddy with the humps removed (the nearest case to a stable one for which the concepts of energy transfer can be made) has only baroclinic transfer. Any stable eddy can be thought of as having exactly canceling barotropic and baroclinic conversion terms (although this interpretation can be misleading). This suggests that stabilization, or near-stabilization, may involve cancellation of baroclinic energy transfer by (negative) barotropic transfer, though further discussion is beyond the scope of this paper.

4. Cold eddies, the β-plane, and quasigeostrophic dynamics

The previous section discussed numerical experiments with warm ring profiles on an f plane. It is of interest to examine the breadth of the result by considering experiments with cold ring profiles and on the β

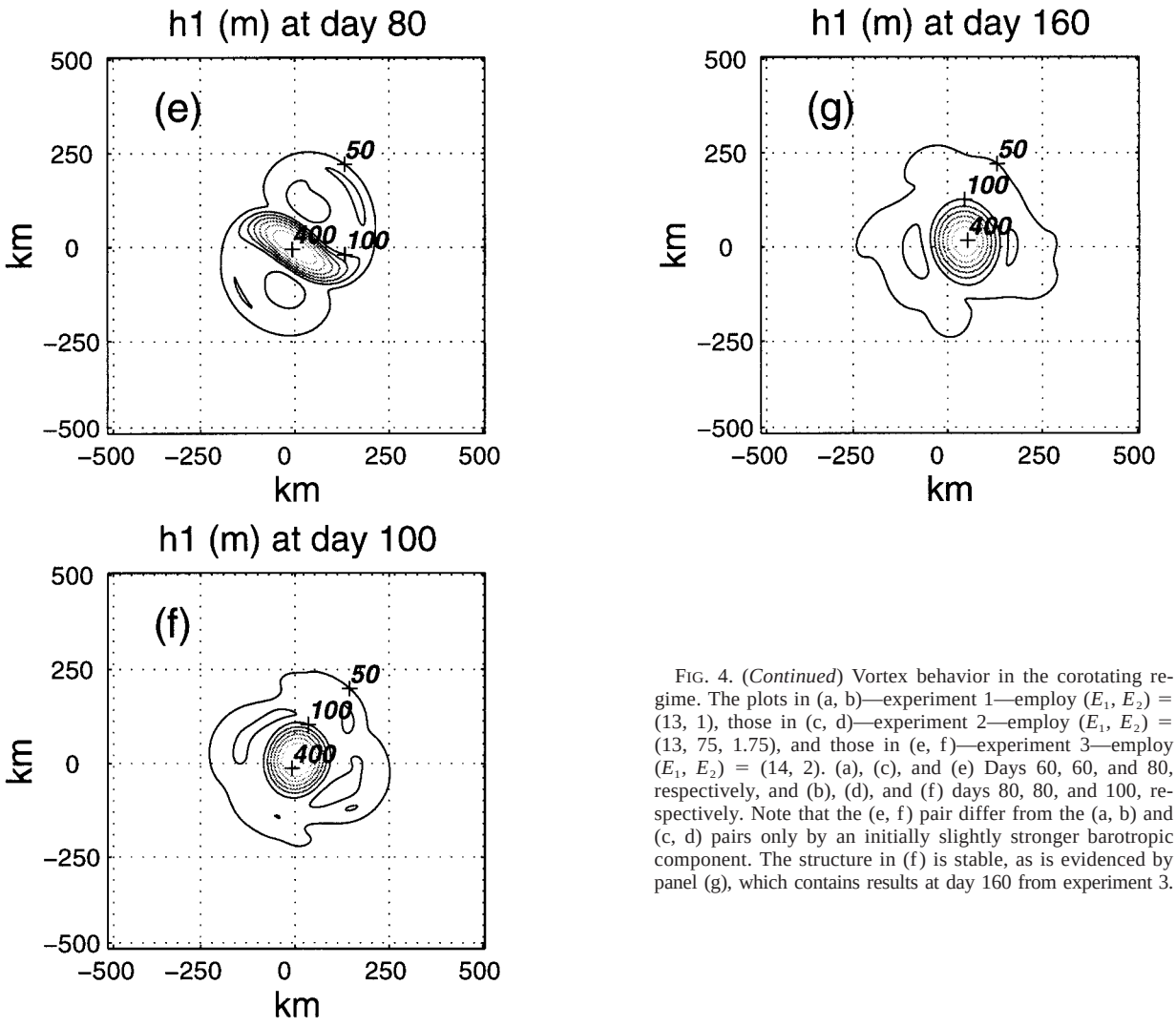

FIG. 4. (*Continued*) Vortex behavior in the corotating regime. The plots in (a, b)—experiment 1—employ $(E_1, E_2) = (13, 1)$, those in (c, d)—experiment 2—employ $(E_1, E_2) = (13, 75, 1.75)$, and those in (e, f)—experiment 3—employ $(E_1, E_2) = (14, 2)$. (a), (c), and (e) Days 60, 60, and 80, respectively, and (b), (d), and (f) days 80, 80, and 100, respectively. Note that the (e, f) pair differ from the (a, b) and (c, d) pairs only by an initially slightly stronger barotropic component. The structure in (f) is stable, as is evidenced by panel (g), which contains results at day 160 from experiment 3.

plane. Both studies are also motivated by observations. Cold rings appear to be as long-lived as warm rings, and of course oceanic rings evolve under the influence of many external effects, β principal among them. Past studies have also considered QG models of rings (e.g., Helfrich and Send 1988; Flierl 1988), so we are motivated to ask how well such dynamics captures the above effect. We here present numerical evidence that cold rings are not stabilized at finite amplitude by corotation, while the stable warm monopoles appearing here on the f plane survive on the β plane. Recall QG dynamics, aside from switching north and south, does not distinguish between warm and cold ring behaviors. Finally, numerical experiments with QG dynamics show that warm ring stabilization is not captured in QG.

a. Cold rings

Our cold core ring experiments use the same exponential profile for the thickness field [see (9)] and the same maximum depth change (480 m) as our warm ring experiments. However, we will use a far-field thickness value for the upper layer of 520 m. Such a value is characteristic of Gulf Stream cold core rings (see the Ring Group 1981) and results in a central ring thickness of 40 m. We will retain our reduced gravity value of 0.0106 m s^{-2}.

We show in Fig. 7 the results of a primitive equation f-plane integration to 20 days of a corotating cold ring initial profile. The experiment shown in this figure involved an eddy seeded with a nonnormal mode perturbation. Specifically, the perturbation came from a mix of the unstable eigenmodes of other eddy profiles, and hence represents an (almost) random perturbation field.

The upper-layer flows are three times stronger than the lower-layer flows, thus this cold ring is comparable to the (18, 6) warm ring case seen in Fig. 3d. The value of viscosity in this experiment was 20 m^2 s^{-1}, and we display the upper-layer thickness field.

Note that the initial ring structure has fragmented into

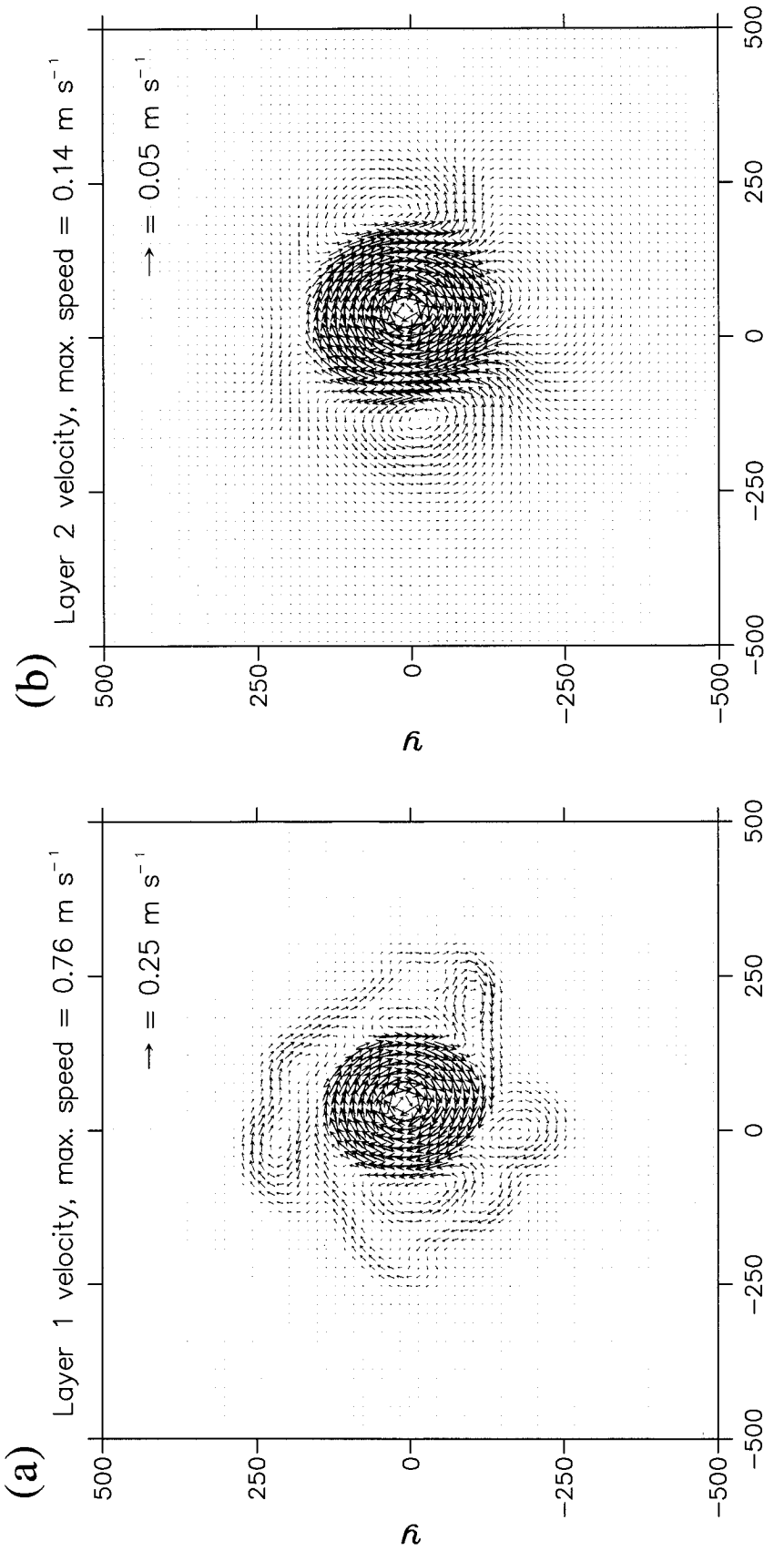

FIG. 5. Velocity plot in (a) layer 1 and (b) layer 2. This corresponds to the day 160 results from experiment 3 shown in Fig. 4. Maximum velocities are indicated on diagrams. Velocity vectors are capped at a maximum of 0.25 m s^{-1} (5a) and 0.05 m s^{-1} (5b), indicated by the scale arrows. Note the cyclones neighboring the anticyclonic vortex, which appear in both layers. Associated with this is a weak thermocline expression, which accounts for the largely barotropic velocity structure. We speculate the suggested underlying barotropic tripole is associated with the stability of the baroclinic monopole.

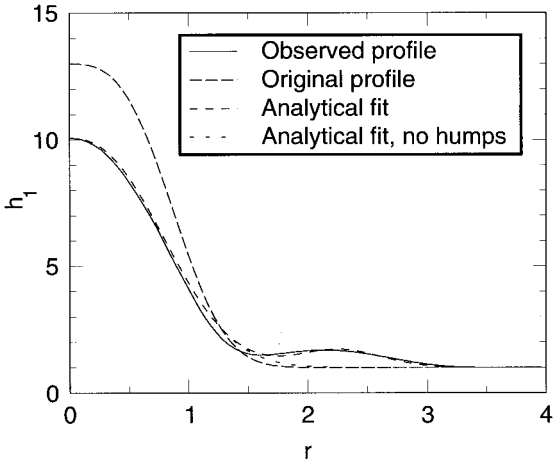

FIG. 6. Upper-layer depth fields for the symmetrized (14, 2) eddy at day 160. The firm line shows the actual depth after symmetrizing, the long dashed line the original (undisturbed) profile, the medium dashed line the analytical fit in the text, and the short dashed line the same fit without the Gaussian riders. All fits lie within one standard error of the symmetrized profile at all points; thus, if the profile were taken from observations, the different profiles would be indistinguishable. As discussed in the text, the stability properties differ strongly, however.

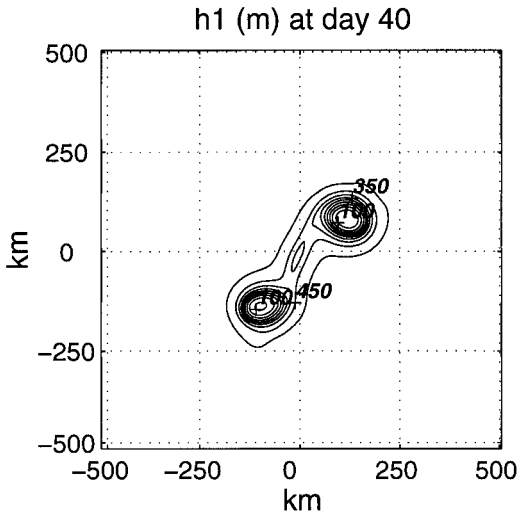

FIG. 7. Cold ring primitive equation results at day 20 from a corotating initial condition corresponding to $(E_1, E_2) = (18, 6)$. The upper-layer thickness field is shown and the values are in meters: CI = 50 m.

two smaller pieces. Investigation of the velocity structure shows that the pieces each consist of dipoles. The subsequent evolution of this structure is that the two parts separate. Hence, this initial structure is identified as effectively unstable, and the experiment demonstrates that cold rings do not experience the same stabilization from a corotating initial state as do warm rings. As a side note, the finite amplitude stability problem here is sensitive to viscosity. An experiment at the typically used 100 $m^2\ s^{-1}$ viscosity value yielded an essentially monopolar cold structure at 100 days (not shown).

b. β-plane experiments

In Fig. 8a, we show the results of a primitive equation warm core ring corotating experiment [using the (18, 6) eddy] on a β plane. [For all our β-plane experiments, $\beta = 2 \times 10^{-11}$ $(m\ s)^{-1}$.] As for the f-plane experiments, the initial eddy was seeded with a small amount of the most unstable eigenmode. The thermocline state at day 100 is shown, from which it is quite clear that the monopolar structure of the initial profile has been preserved. Note the main center with a thermocline displacement in excess of 400 m. Figure 8b shows for comparison the thermocline profile at day 100 of a warm ring β-plane experiment with the (6, −6) eddy, similarly seeded with its most unstable eigenmode, in which it is clear the monopolar integrity of the initial, large ring has been lost. In its place are two smaller eddies of roughly 200-m net isopycnal displacement.

The vector diagrams in Fig. 8c show the velocity field from both the upper and lower layers for the corotating case in Fig. 8a. The region shown corresponds to the vicinity of the monopole in Fig. 8a and data from every third point are plotted. The figure demonstrates that the structure has retained a barotropic component as far out as day 100. This is notable because one might intuitively expect that β and the attendant barotropic radiation caused by it would erode the net barotropic flow. These results suggest rather that the flow and thermocline structure interrupts barotropic radiation from the vortex. We further speculate that this allows the ring to retain its coherence.

In view of the f-plane instability of the initial cold ring profiles, we do not show any β-plane experiments with cold eddies.

c. Quasigeostrophic experiments

In our quasigeostrophic experiments, it is necessary to differentiate between warm and cold core experiments because of the above differences in far-field thicknesses. Warm core ring experiments employ an upper-layer thickness of 40 m, while including a 480-m thickness anomaly. Cold core ring experiments use a far field of 520 m and a 480-m elevation of the interface. While we do not pretend that these profiles fit within the parametric restrictions of quasigeostrophic theory, we are nonetheless interested in whether the qualitative stabilization effect of deep flow can be captured. Note, the biggest dynamical difference between the primitive equation and QG experiments in these cases reduces to the artificial suppression of the layer thickness in the QG case.

For this set of experiments, we employed the Holland (1978) quasigeostrophic model in a two-layer configuration. The spatial resolution was the same as our primitive equation experiments, that is, 5 km, and the domain

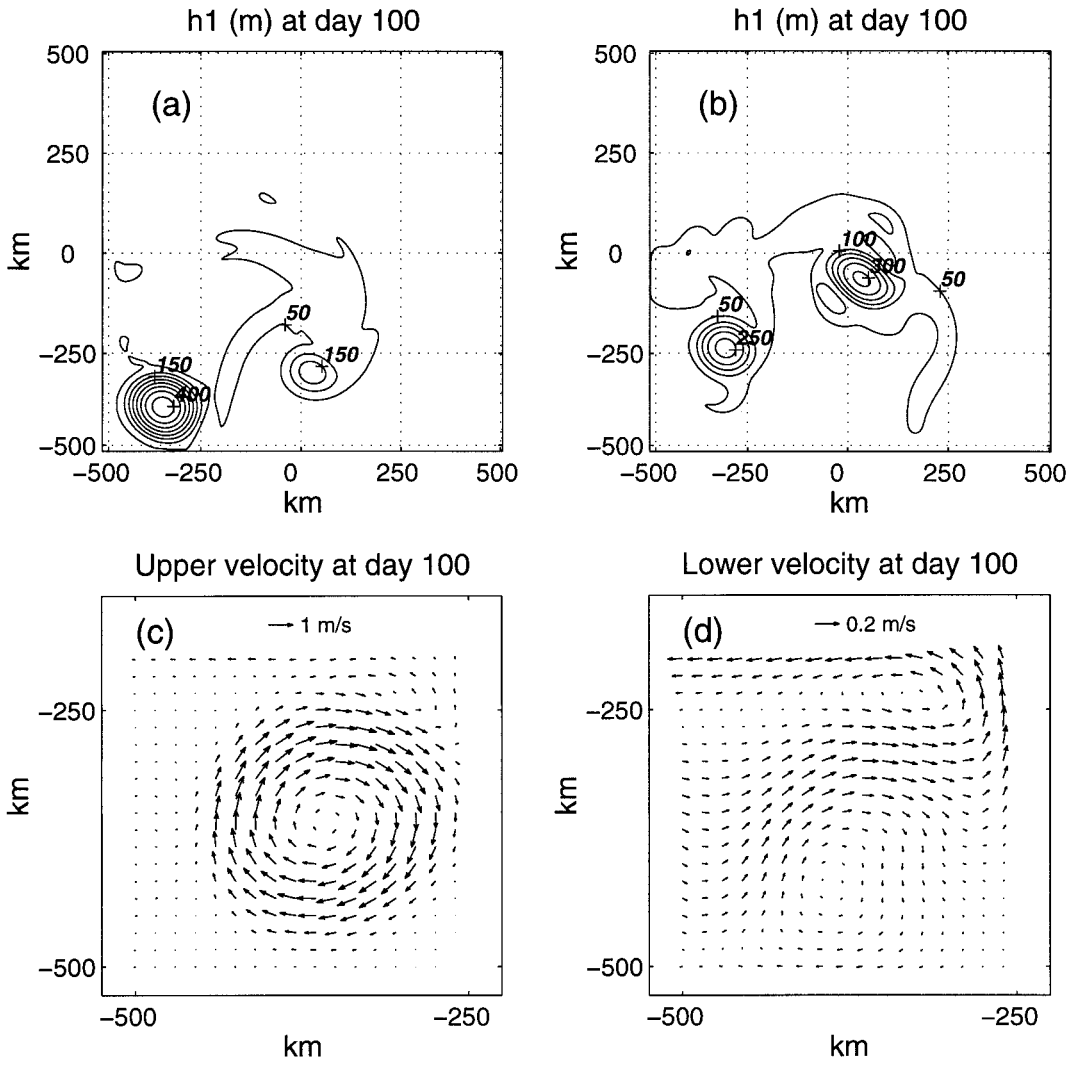

FIG. 8. Primitive equation β-plane experiments. (a) The upper-layer thickness field from a warm ring corotating initial profile corresponding to (18, 6) is shown at day 100. (b) As in (a) but for a warm ring counterrotating profile corresponding to (6, −6); CI = 50 m in both. (c) Upper- and (d) lower-layer vector velocity plots from the region of the dominant anticyclone in (a), showing the retention at day 100 of a barotropic mode by the ring.

size was 1000 km in both dimensions. A biharmonic viscous operator was used, with the relevant coefficient set to either -1×10^6 m^4 s^{-1} or -1×10^8 m^4 s^{-1}. (In a small number of cases, we have performed experiments using these two viscosity values on the same initial condition. The results were always found to be virtually identical, suggesting viscosity was not playing a significant role.) The same thermocline profile and amplitude as in the primitive equation experiments were used.

Figures 9a,b show the results of two f-plane warm ring experiments. Again, the experiments are differentiated by their respective depth-integrated flows and correspond to the (18, 6) eddy in (a) and the (6, −6) eddy in (b). Both eddies were seeded with the thickness perturbations from the most unstable primitive equation eigenmodes associated with their (E_1, E_2) values. The actual most unstable QG eigenmode differs from this, making these nonnormal mode perturbations.

The results in (a) and (b) are both from day 40. This distinction in time relative to that used in the primitive equation results appearing in Fig. 4 (day 100 for the corotating ring) emphasizes that the overall instability in the QG case is quantitatively much different. Further, the corotating case in (a) shows that the initial state is degenerating into two dipoles, similar to the counterrotating case in (b). The appearance of different instability growth rates between the co- and counterrotating cases [as evidenced by the much advanced degeneration of the vortex in (b)] is consistent with the results of Helfrich and Send (1988) and Flierl (1988). However, the comparison of the corotating results with those in

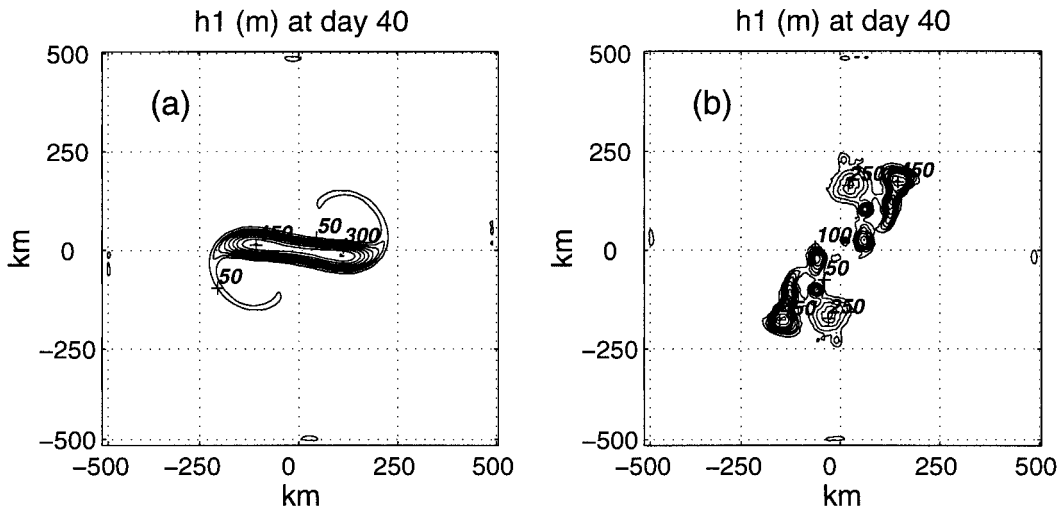

FIG. 9. Quasigeostrophic f-plane experiments. (a) The upper-layer thickness anomaly from a corotating (18, 6) warm ring initial profile at day 40. (b) As in (a) but for a counterrotating initial profile corresponding to (6, −6) at day 40; CI = 50 m in both.

Fig. 3d demonstrates a qualitative difference from the primitive equation case. We again mention that increases in the viscosity parameters beyond the values mentioned above could stabilize the corotating QG case, while leaving the counterrotating case unstable. However, even then, β-plane experiments demonstrated that the QG corotating eddy was unable to retain its coherent structure.

Quasigeostrophic experiments with f-plane cold ring initial conditions were found to be unstable, similar to the primitive equation results. None are shown here.

5. Discussion

The vortex stability problem has been studied numerically. We have presented evidence that corotating warm monopolar vortices tend to stay as monopoles much more effectively than do either compensated or counterrotating monopolar vortices. This holds on the β plane and fails to be captured by QG dynamics. Our main result is consistent with the hypothesis forwarded in Dewar and Killworth (1995) that the barotropic component of a vortex plays a significant role in determining its overall stability. Further, it was suggested that corotation lent stability to a given warm baroclinic eddy structure, again consistent with present results.

On the other hand, the character of these solutions and the nature of the vortex stability differ from the earlier DK results. The term stability is interpreted in a general sense to imply the resulting state is mainly monopolar and ''near'' the initial state. The linear instability of the basic state is thus somewhat irrelevant to the survival of the monopole. It is also curious, and not understood, why this appears to be a property of corotating warm structures. A tendency for the system to equilibrate in a weak tripolar configuration was, however, noted.

We have been motivated to study this problem by the now widely accepted observational result that apparently monopolar vortices are long-lived. Further, a strong argument can be made that this behavior is generic in ocean vortices. Given this dominant signal, the dynamical underpinnings for it become of interest. It is, however, fair to say that oceanic vortex stability is not yet understood. The results presented in this paper support the idea that warm rings with a favorable barotropic component can retain their monopolar nature. Since many oceanic vortex observations hint at the presence of coherent strong deep flows in their vicinity, we continue to speculate that the mechanism discussed in this paper is in operation in the open ocean, and encourage direct velocity observations in deep water within rings. On the other hand, the observed stability of cold rings remains a dynamical enigma.

Acknowledgments. WKD is supported by NASA Grants NAGW-4883 and NAG5-4613 and NSF Grants OCE-9401977 and OCE-9617728. Sheila Heseltine prepared the manuscript. Ms. Jane Jimeian assisted in computational issues and figure preparation. The authors would like to thank two anonymous reviewers for many helpful comments.

REFERENCES

Benilov, E., D. Broutman, and E. Kuznetsova, 1997: On the stability of large-amplitude vortices in a continuously stratified fluid on the f-plane, *J. Fluid Mech.,* **355,** 139–162.

Bleck, R., and E. P. Chassignet, 1994: Simulating the oceanic circulation with isopycnic-coordinate models. *The Oceans: Physical–Chemical Dynamics and Human Impact,* S. K. Majumdar,

E. W. Miller, G. S. Forbes, R. F. Schmalz, and A. A. Panah, Eds., The Pennsylvania Academy of Science, 17–39.

Brown, O. B., P. C. Cornillon, S. R. Emmerson, and H. M. Carle, 1986: Gulf Stream warm rings: a statistical study of their behavior. *Deep-Sea Res.*, **33,** 1459–1473.

Carton, X., and J. McWilliams, 1989: Barotropic and baroclinic instabilities of axisymmetric vortices in a quasigeostrophic model. *Mesoscale/Synoptic Coherent Structures in Geophysical Turbulence*, J. C. Nihoul and B. Jamart, Eds., Elsevier, 841 pp.

Chassignet, E. P., 1990: Motion and evolution of oceanic rings in a numerical model and in observations. *J. Geophys. Res.*, **95,** 22 121–22 140.

Dewar, W. K., and P. D. Killworth, 1995: On the stability of oceanic rings, *J. Phys. Oceanogr.*, **25,** 1467–1487.

Flierl, G. R., 1988: On the instability of geostrophic vortices. *J. Fluid Mech.*, **197,** 349–388.

Gordon, A. L., and W. F. Haxby, 1990: Agulhas eddies invade the South Atlantic: Evidence from Geosat altimeter and shipboard conductivity–temperature–depth survey, *J. Geophys. Res.*, **95,** 3117–3125.

Helfrich, K. R., and U. Send, 1988: Finite-amplitude evolution of two-layer geostrophic vortices. *J. Fluid Mech.*, **197,** 331–348.

Holland, W., 1978: The role of mesoscale eddies in the general circulation of the ocean-numerical experiments using a wind-driven quasi-geostrophic model, *J. Phys. Oceanogr.*, **8,** 363–392.

Hooker, S. B., J. W. Brown, A. D. Kirwan, Jr., G. J. Lindemann, and R. P. Mied, 1995: Kinematics of a warm-core dipole ring, *J. Geophys. Res.*, **100,** 24 797–24 809.

Ikeda, M., 1981: Instability and splitting of mesoscale rings using a two-layer quasigeostrophic model on an f-plane. *J. Phys. Oceanogr.*, **11,** 987–998.

Kennelly, M., R. H. Evans, and T. M. Joyce, 1985: Small-scale cyclones on the periphery of a Gulf Stream warm-core ring, *J. Geophys. Res.*, **90,** 8845–8857.

Killworth, P. D., 1980: Barotropic and baroclinic instability in rotating stratified fluids, *Dyn. Atmos. Ocean.*, **4,** 143–184.

——, 1992: An equivalent-barotropic mode in the Fine Resolution Antarctic Model, *J. Phys. Oceanogr.*, **22,** 1379–1387.

——, J. R. Blundell, and W. K. Dewar, 1997: Primitive-equation instability of wide oceanic rings. I. Linear theory, *J. Phys. Oceanogr.*, **27,** 941–962.

Kloosterziel, R. C., and G. Van Heijst, 1989: On tripolar vortices. *Mesoscale/Synoptic Coherent Structures in Geophysical Turbulence*, J. C. Nihoul and B. Jamart, Eds., Elsevier, 841 pp.

Lai, D. Y., and P. L. Richardson, 1977: Distribution and movement of Gulf Stream rings. *J. Phys. Oceanogr.*, **7,** 670–683.

Olson, D. B., and R. H. Evans, 1986: Rings of the Agulhas Current. *Deep–Sea Res.*, **33,** 27–42.

——, R. W. Schmitt, M. Kennelly, and T. M. Joyce, 1985: A two-layer diagnostic model of the long-term physical evolution of warm-core ring 82B. *J. Geophys. Res.*, **90,** 8813–8822.

Paldor, N., and D. Nof, 1990: Linear instability of an anticyclonic vortex in a two-layer ocean, *J. Geophys. Res.*, **95,** 18 075–18 079.

Ripa, P., 1992: Instability of a solid-body rotating vortex in a two-layer model. *J. Fluid Mech.*, **242,** 395–417.

The Ring Group, 1981: Gulf Stream cold core rings: Their physics, chemistry and biology. *Science*, **212,** 1091–1100.